

Evidence for Quantized and Variable Redshifts in the Cosmic Background Rest Frame

W. G. Tift
Steward Observatory, University of Arizona
Tucson, Arizona 85721

Abstract

Evidence is presented for redshift quantization and variability as detected in global studies done in the rest frame of the cosmic background radiation. Quantization is strong and consistent with predictions derived from concepts associated with multidimensional time. Nine different families of periods are possible but certain ones are more likely to occur. The most basic family contains previously well known periods of 73 and 36 km s^{-1} along with still shorter harmonics at 18.3 and 9.15 km s^{-1} . Several approaches to evaluating the significance of quantization are employed and the dependence of quantization on redshift, the width and shape of 21 cm profiles, morphology, and other parameters is discussed. Common properties between samples are investigated to define several basic classes of galaxies. Quantization is found to be consistently optimized for a transformation vertex very close to the vertex defined by the cosmic background dipole component. The relationship between the cosmocentric and galactocentric rest frames is discussed.

1. Introduction

The objective of this paper is to present current evidence for global redshift quantization and to examine some of its properties. By global redshift quantization we mean that the redshifts of homogeneous classes of galaxies from all over the sky contain specific periods when viewed in an appropriate rest frame; the redshift is not a continuous variable as expected from the standard Doppler interpretation. Work prior to 1992 is summarized in a recent review (Tift 1995a). We will not discuss the background or cosmological models here. Early discussions of cosmology are contained in Tift (1995b) and Tift, Cocke & DeVito (1996). A current empirical model is discussed elsewhere (Tift 1996a).

Two major advances in quantization work occurred in 1992 and early 1993. The first was the recognition that the primary reference frame for global quantization appears to be the 3 degree cosmic background radiation rest frame (Cocke & Tift 1996). The second was the recognition of a possible model (Lehto, 1990), which permits the prediction of redshift periods in terms of the Planck energy. This model, which views time as three dimensional, permits one to connect the structure of matter to redshift effects and cosmology. We will refer to it here as the temporal model.

The original work on global redshift quantization used a galactic center rest frame (Tift 1978a,b Tift & Cocke 1984). Quantization was found for galaxies with the widest and narrowest 21 cm profiles, but was not apparent for the majority of intermediate objects. By transforming to the CBR rest frame it is now possible to work with all types of galaxies. It is our impression that there is a fundamental effect in the cosmic frame. The presence of this effect can induce large non-random effects in other rest frames. This seems to be especially true for the galactic center rest frame where Guthrie and Napier (1991, 1996) have independently confirmed periodicities. We will compare rest frames further later in this paper.

Prior to 1993 redshift periods were known only empirically. The periods appeared to be related by simple factors to a period near 72 km s^{-1} . One of the most important periods is near 36 km s^{-1} . Any ambiguity introduced by uncertainty in the periods has now been largely eliminated by using the precise predicted periods given by the 3-d temporal model. A main thrust of this paper is to show how accurately these periods fit observations. Although the first demonstration of the importance of the CBR reference frame used the old empirical periods, the combination of the CBR rest frame and the 3-d temporal concepts now permits a simultaneous demonstration of the match to predicted periods and the presence of a consistent CBR vertex. A detailed discussion is contained in Tift (1996b).

From the start of quantization studies it has been apparent that redshift periods and phasings depend upon properties of the galaxies themselves. It is essential to work with accurate homogeneous data sets. Quantization may be seen in relatively unrestricted samples, but periods and rest frame transformations can be distorted. Accuracy requirements has largely limited the work to 21 cm redshifts where measures at high signal-to-noise levels achieve sub km s^{-1} precision (Tift & Cocke 1988, Tift 1990). Using 21 cm data, sample homogeneity has been obtained primarily by sorting data according redshift, 21 cm profile width, W , and in some cases profile shape or asymmetry, A . Standard morphology, especially the t index, is also used. Low quality data is generally removed using signal-to-noise, S/N , or flux-to-width, F/W , ratios. The latter index also separates samples by luminosity in deep redshift surveys. Studies of 21 cm redshift precision led to the discovery of apparent redshift variability; redshifts seem to shift rapidly within the periodic pattern. Because of this possible effect redshift sources are rarely combined, and samples are limited to time intervals as short as possible.

The most recent transformation used to refer redshifts to the galactic center is $(232.2, -36.6, 0.9) \text{ km s}^{-1}$, where the numbers are the transverse, radial, and perpendicular components in galactic coordinates. This transformation is now usually applied relativistically. Older values of this transformation rarely differ by more than 1 or 2 km s^{-1} . The most recent CBR transformation is $(-243, -31, 275)$. It is typically applied as a Galilean transformation sequential with a relativistic galactic center transformation. Alternatively a direct Galilean CBR transformation of $(-241.7, -30.8, 275.1)$ has been applied to heliocentric redshifts. The small differences produce negligible effects except at very short periods. One result which seems increasingly clear is that a relativistic transformation to the CBR is not correct. There is a need to do a more definitive study of the vertices and the form of the transformation, but the present uncertainties do not affect any important conclusions.

The association of redshift quantization with the CBR reference frame provides one link between the effect and cosmology. A second link is provided by nonlinearity in the periodicity with lookback time. Before redshifts are analyzed a correction is applied according to

$$V_{corr} = 4c[(1+z)^{1/4} - 1] + \dots \quad (1)$$

Higher terms in the expression are a function of q_0 , and cancel out for $q_0 = 1/2$. This equation is derived in Tift (1991). The relevance of the equation, and a demonstration that $q_0 = 1/2$ is appropriate, is given in Tift (1996b). The correction is of no consequence for long periods and local galaxies. It becomes important for short periods and high redshifts.

2. The Periodicity Rule

Lehto (1990) attempted to describe basic properties of matter beginning with a minimum fundamental unit of time, the Planck time, and subsequently expanding it into observable time intervals by a doubling process. The Planck time is.

$$t_0 = \frac{1}{\nu_0} = \sqrt{\frac{hG}{c^5}} = 1.3506 \times 10^{-43} \text{ s}, \quad (2)$$

where h is Planck's constant, G the gravitational constant, and c the speed of light. ν_0 is a corresponding maximum frequency which defines a maximum unit energy.

$$E_0 = h\nu_0 = \frac{h}{t_0} = 4.905 \times 10^{16} \text{ erg}, \quad (3)$$

and an associated maximum unit mass

$$m_0 = \frac{E_0}{c^2} = 5.458 \times 10^{-5} \text{ gm}. \quad (4)$$

These units alone are sufficient to construct a model describing the properties of fundamental particles and redshift periodicities. Only time and energy, in energy or mass form, is involved. This is all that is in fact assumed in the current temporal model.

In his initial work Lehto (1990) included spatial units. There could be a minimum spatial interval, the Planck distance

$$r_0 = ct_0 = 4.049 \times 10^{-33} \text{ cm}. \quad (5)$$

Recent work in quantum gravity has suggested that such finite minimum spatial intervals could be a property of space. In a discrete space-time lattice structure, if velocity is defined as allowed distances divided by allowed times, the basic unit of velocity is

$$v_0 = \frac{r_0}{t_0} = c. \quad (6)$$

As noted above spatial quantization is not required by redshift quantization, and even if correct may not explain quantization in observed velocities which are projections of total velocities. In the present temporal model space is assumed to be continuous.

Given basic units, Lehto assumed that a period doubling process, known to operate in various chaotic decay processes, could provide a mechanism to extend the Planck units into the observable domain. In the simplest period doubling process observable values are related to the fundamental by a factor $2^{\pm D}$, where D is the number of doublings. If such a scheme is operating, observed fundamental masses, energies, etc will be related by simple integer powers of 2. What Lehto found was that exponents appeared to concentrate at $1/3$ integer values. He interpreted this to imply that time could be three-dimensional. One dimensional perceived time is related to a three dimensional volume in temporal 3-space. Volume doubling is reduced to one dimension by taking cube roots; perceived time is a scalar with sign and magnitude only. Lehto wrote perceived times as

$$t = t_0 2^{\frac{k}{3}} = t_0 2^{\frac{N_x + N_y + N_z}{3}} = t_0 2^{\frac{3D+M}{3}}. \quad (7)$$

N values are individual axial doublings, D is the net doubling and M is a temporal fraction, 0, 1 or 2. The D, M notation distinguishes doubling families; values with constant M are related by powers of two. There are three doubling sequences.

Equation (7), combined with Equations (3) and (4), permits calculation of particle masses and particle pair energies. Lehto was able to show that the mass corresponding to $L = 227$ is equivalent to the electron mass within the uncertainty in the values of the physical constants used to determine t_0 . Recent extensions of the temporal concept have been able to model most of the basic stable particles and forces (Tift & Lehto 1996).

Equation (7) assumes that volumes follow a doubling rule where all three axes scale by $2^{1/3}$ simultaneously. If we remove this restriction time intervals can grow in steps of $2^{1/9}$

$$t = t_0 2^{\frac{9D+T}{9}}. \quad (8)$$

The integer T ranges from 0 to 8. There are 9 period doubling series in this representation.

Possible redshifts, in velocity units, are given by

$$v = P = c 2^{-\frac{9D+T}{9}}. \quad (9)$$

Because velocities for successive D values differ by the velocity values themselves, this equation also represents all first order velocity differences, hence possible redshift periods, P . This is the periodicity rule which is found to fit observed redshift periods very well. The basic $T = 0$ sequence contains periods of 73.2 and 36.6 km s^{-1} , which closely match the empirical periods discovered in the 70s. Although the 3-d temporal model has proven to be quite fruitful, this paper is intended primarily to show how well equation (9) fits redshift data without regard to any interpretation of the equation.

3. First Tests, Virgo Dwarfs

Certain classes of local galaxies show periodic redshift patterns in the galactic center rest frame; the patterns are not seen in 21 cm data on Virgo cluster dwarf galaxies by Hoffmann et al (1987). The first tests of the CBR association used primarily local galaxies (Cocke & Tift 1996). The Virgo galaxies provided the first test combining the CBR association with periodicity predictions of equation (9). The results were striking; clear periodicities matching the predictions were present. We will cite some examples and summary statistics here; details are given in Tift (1996b). Several techniques have been used to evaluate significance, but the simplest way to show the periodicities is by spectral power analysis. As used here the average power and power dispersion for random data should be close to unity. The probability of finding a given power at a single specified frequency is approximately inversely exponential in the power. For a more detailed discussion see Cocke, DeVito & Pitucco (1996).

Figure 1 contains power spectra for galaxies falling within different overlapping intervals of 21 cm profile width, W . Three periods stand out; two match the original 36 and 72 km s^{-1} periods. Essentially all the significant peaks match periods predicted by equation (9); predictions are shown with vertical lines. Table 1 summarizes properties of the three main periods. The peak power and the ratio of the period at peak power to the predicted period are given as a function of profile width. The ratio is henceforth called the pk/per ratio. The following statements summarize findings and anticipate results to be brought out later:

- 1) As W is varied, power may shift between periods, especially harmonics within one T family, but the peaks closely track the predicted periods. Width adjustment varies the power but does *not* 'tune' periods.
- 1a) Distinct phase shifts within the same period occur near certain profile widths. This is not apparent in the dwarf-dominated Virgo sample but will be shown later. Certain periods or T values tend to associate with particular morphology and profile width intervals.
- 1b) Redshifts generally concentrate in absolute phase around simple common fractions of the periods. Concentrations are not randomly spread in phase. This is again most easily shown with later samples.

The association of redshift quantization with the CBR reference frame provides one link between the effect and cosmology. A second link is provided by nonlinearity in the periodicity with lookback time. Before redshifts are analyzed a correction is applied according to

$$V_{corr} = 4c[(1+z)^{1/4} - 1] + \dots \quad (1)$$

Higher terms in the expression are a function of q_0 , and cancel out for $q_0 = 1/2$. This equation is derived in Tift (1991). The relevance of the equation, and a demonstration that $q_0 = 1/2$ is appropriate, is given in Tift (1996b). The correction is of no consequence for long periods and local galaxies. It becomes important for short periods and high redshifts.

2. The Periodicity Rule

Lehto (1990) attempted to describe basic properties of matter beginning with a minimum fundamental unit of time, the Planck time, and subsequently expanding it into observable time intervals by a doubling process. The Planck time is.

$$t_0 = \frac{1}{\nu_0} = \sqrt{\frac{hG}{c^5}} = 1.3506 \times 10^{-43} \text{ s}, \quad (2)$$

where h is Planck's constant, G the gravitational constant, and c the speed of light. ν_0 is a corresponding maximum frequency which defines a maximum unit energy.

$$E_0 = h\nu_0 = \frac{h}{t_0} = 4.905 \times 10^{16} \text{ erg}, \quad (3)$$

and an associated maximum unit mass

$$m_0 = \frac{E_0}{c^2} = 5.458 \times 10^{-5} \text{ gm}. \quad (4)$$

These units alone are sufficient to construct a model describing the properties of fundamental particles and redshift periodicities. Only time and energy, in energy or mass form, is involved. This is all that is in fact assumed in the current temporal model.

In his initial work Lehto (1990) included spatial units. There could be a minimum spatial interval, the Planck distance

$$r_0 = ct_0 = 4.049 \times 10^{-33} \text{ cm}. \quad (5)$$

Recent work in quantum gravity has suggested that such finite minimum spatial intervals could be a property of space. In a discrete space-time lattice structure, if velocity is defined as allowed distances divided by allowed times, the basic unit of velocity is

$$v_0 = \frac{r_0}{t_0} = c. \quad (6)$$

As noted above spatial quantization is not required by redshift quantization, and even if correct may not explain quantization in observed velocities which are projections of total velocities. In the present temporal model space is assumed to be continuous.

Given basic units, Lehto assumed that a period doubling process, known to operate in various chaotic decay processes, could provide a mechanism to extend the Planck units into the observable domain. In the simplest period doubling process observable values are related to the fundamental by a factor $2^{\pm D}$, where D is the number of doublings. If such a scheme is operating, observed fundamental masses, energies, etc will be related by simple integer powers of 2. What Lehto found was that exponents appeared to concentrate at $1/3$ integer values. He interpreted this to imply that time could be three-dimensional. One dimensional perceived time is related to a three dimensional volume in temporal 3-space. Volume doubling is reduced to one dimension by taking cube roots; perceived time is a scalar with sign and magnitude only. Lehto wrote perceived times as

$$t = t_0 2^{\frac{k}{3}} = t_0 2^{\frac{N_x + N_y + N_z}{3}} = t_0 2^{\frac{3D+M}{3}}. \quad (7)$$

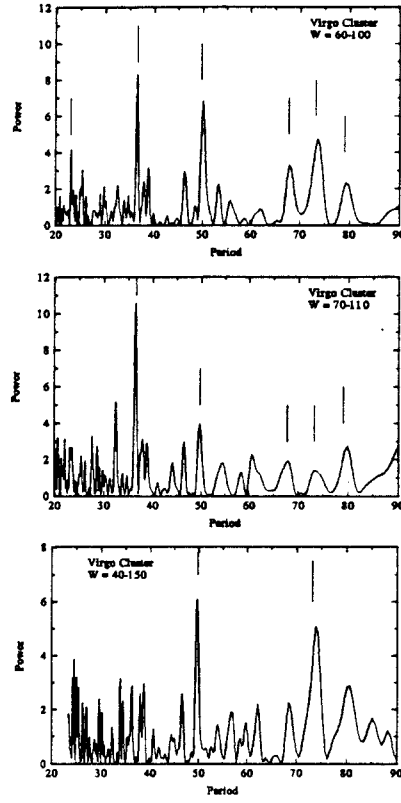


Fig. 1) Power spectra of the Virgo region sample subdivided into 21 km profile width intervals, W , in km s^{-1} . The abscissa is redshift period in km s^{-1} . Vertical lines mark predicted periods. The power at a given period depends upon the profile width interval utilized but the locations of the peaks do not.

TABLE 1
Spectral Power Data for Virgo

Width km s^{-1}	Pk Pow $P=73.1916$	Pk/Per	Pk Pow $P=36.5958$	Pk/Per	Pk Pow $P=49.7992$	Pk/Per
50- 90	5.6	1.0004	< 4	...	7.7	1.0084
60-100	4.2	1.0029	8.3	0.9966	7.1	1.0033
70-110	< 4	...	9.8	0.9947	4.1	0.9980
100-250	4.8	0.9912
60-125	< 4	...	5.0	0.9926	7.1	0.9979
40-150	5.1	1.0111	< 4	...	6.3	0.9975
All	4.0	1.0126	< 4	...	6.1	0.9970

2) The pk/per ratio is a measure of the quality of fit to the set of predicted periods. The ratio between adjacent predicted values is 1.0801, the ninth root of two. Power peaks concentrate strongly around 1.00 and avoid values near 1.04 midway between predictions.

3) Periods in the basic $T = 0$ family are almost always dominant. Periods are not distributed randomly in T ; two cube root families, $T = 0$ and 6, dominate. Some ninth-root families tend to occur simultaneously with the dominant families, $T = 1, 5$ and 7 being the most important. The 49.8 km s^{-1} Virgo period has $T = 5$.

Figure 2 shows the mapping of power, at the 36.6 km s^{-1} predicted peak, around the expected values of the transverse and radial transformation components appropriate to the CBR and galactic center rest frames. The small box is the COBE error box for the CBR vertex. X symbols mark the adopted quantization vertices. The Virgo galaxies, not being widely spread on the sky, show a broad power concentration associated with the CBR and not the galactic center. Subsequent examples will show the CBR association with much greater resolution. The relationship between the rest frames will be briefly discussed later in the paper.

4) Power at predicted periods is maximized when redshifts are transformed to a rest frame close to the COBE CBR vertex. The radial component is typically slightly more negative than the COBE value.

The significance of the periodicities and the match to equation (9) has been evaluated three different ways. The fact that the single most prominent power peak occurs at the previously well known period near 36 km s^{-1} with a power of 10 is significant by itself. Even if we allow that about 20 predicted periods fall in the range studied, and degrade significance by that factor, a match at any period at power 10 has a likelihood of accidental occurrence below the 0.001 level. Since at least three of the periods are matched above power 6 and no high power peaks fail to match periods, it is difficult to escape the conclusion that equation (9) well describes real periodicities present in the CBR rest frame.

Since questions have been raised about using extreme power values to estimate likelihoods we have used a binomial test to evaluate the degree to which all peaks above power 4 fit predicted periods. When we search the power spectra for all the different profile width intervals in the period range from 20 to 100 km s^{-1} we are able to identify 14 independent power peaks reaching above 4.0. Although the fits vary slightly with profile width, 8 of the 14 peaks lie at or within 0.005 of unity in the pk/per fitting index. Since the index should be uniformly populated between 1.00 ± 0.04 for a random distribution of power, the probability of falling within 0.005 of unity is $1/8$. The likelihood of finding 8 or more fits in 14 trials within this tolerance is 8×10^{-5} . The likelihood of finding more than 4 fits is already < 0.05 .

A third test makes use of the unit mean and dispersion in power expected for a random distribution. Eight sets of periods were generated by scaling the predicted periods by factors 0.97, 0.98, ..., 1.04 to cover the range between predicted periods. The mean and dispersion in power was then found for the 25 periods between 23 and 150 km s^{-1} using three data sets in the 60 to 100 km s^{-1} width range. Figure 3 shows the result as a function of the scaling factor. The distributions peak sharply at 1.00, the predicted period set. Comparing the mean and dispersion at 1.00 with the values midway between the predicted periods using a Student's t test yields $t = 4.1$, or about a 10^{-4} likelihood that they arise from the same parent population. Using power levels, peak locations, or the power distributions we find consistent significant results. The Virgo dwarf galaxies contain periodicities uniquely consistent with equation (9) when viewed from the CBR rest frame.

We should perhaps emphasize here how the third test confirms the statement in conclusion 1 that adjusting profile width intervals does not arbitrarily tune periods. If this were so then we should have found many intermediate periods. Real periods should shift only slightly and show power variation according to their actual profile width dependence. This is what we observe. To test for tuning of spurious periods one must use periods which are not predicted. The third test shows that such periods are not found in significant numbers. Arbitrary periods are found at less than random expected levels since the redshift distribution is not random, it contains stable predicted periods.

4. A Second Sample, The Perseus Supercluster

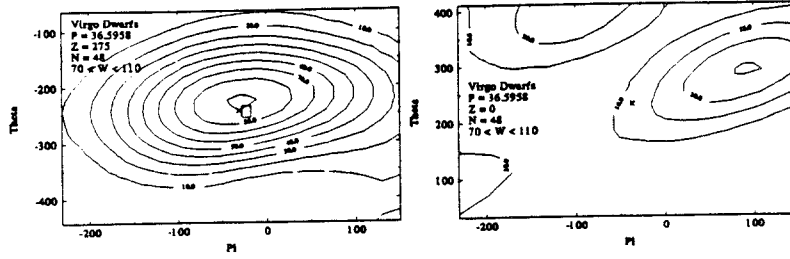


Fig. 2) Contour diagrams of power, at the 36.6 km s^{-1} period, for a sample of Virgo cluster galaxies. W is profile width in km s^{-1} . Power is shown scaled by a factor of 10. The axes are the θ and π components, in km s^{-1} , of the vector used to transform to the CBR rest frame (left) or galactic center (right). Each diagram refers to a constant Z component as indicated. The box is the COBE error box for the CBR dipole vertex. The x in each frame is the approximate location of the rest frame vertex based upon previous quantization studies. The Virgo periodicities associate with the CBR vertex, but not with the galactic center.

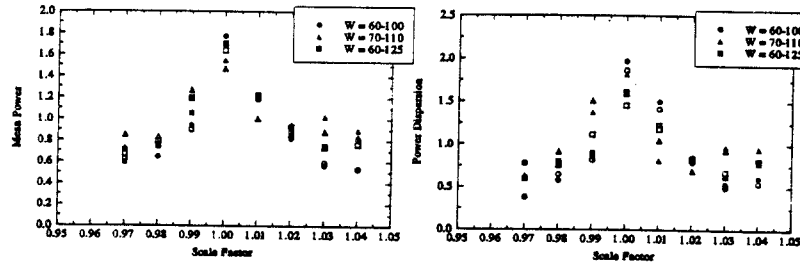


Fig. 3) Mean power and power dispersion for 25 periods between 23 and 146 km s^{-1} . Symbols distinguish profile width subsets of Virgo galaxies; W is in km s^{-1} . Samples with open symbols cover the complete redshift range; samples with filled symbols omit redshifts smaller than 500 km s^{-1} . Power is measured at points obtained by scaling the predicted periods by the scale factor on the abscissa. Power and dispersion are maximized at the predicted periods and drop as sampling points move away from predictions.

As a second sample for study we use redshifts from the deep Arecibo survey of the Perseus supercluster from Giovanelli and Haynes (1985, 1989). There is a special reason for this choice. A common criticism of periodicity studies is that parameters are adjusted to optimize power and period fits; in the first Perseus samples we shall discuss, all parameters were set prior to the discovery of the ninth-root rule. No optimizing was done; details are given in Tift (1996b). The samples were defined in older studies. In 1984 Tift & Cocke (1984) found that local galaxies with 21 cm profiles wider than about 420 km s^{-1} contained a 36 km s^{-1} galactocentric periodicity. Martin Croasdale (1989) generally verified this using independent data, some of which came from the 1985 Perseus survey. To examine and extend Croasdale's work the 154 galaxies with unblended 21 cm profiles wider than 400 km s^{-1} were compiled from both Perseus region studies. Only 22 of the galaxies are in common with Croasdale.

This ready-made sample was used in 1992 in one of the first studies of the CBR association, prior to any knowledge of equation (9). 73 galaxies with $S/N < 4$ were set aside as being of lower quality. Using the 81 best redshifts it was noted that galaxies with small flux-to-width ratios contained a 36.05 km s^{-1} period which appeared to associate with the CBR rest frame. The F/W ratio provides a rough luminosity distinction. Using this distinction the 81 galaxies were divided into 53 with $F/W < 0.01$ and 28 with $F/W > 0.01$ to roughly optimize the 36.05 km s^{-1} periodicity; this period is, however, *not* one of the periods predicted later by equation (9) and is actually a misfit. By defining the samples using this period we introduce some sample homogeneity but no bias relating to the presence or absence of the periods which were predicted later.

Figure 4 shows redshift phase, plotted in a double cycle to show periodic clumping, for the 81 galaxies with $S/N > 4$. The period used is the predicted $36.5859 T = 0$ period; The abscissa is F/W . The right hand frame shows a section of the 53 point power spectrum at longer periods. Table 2 summarizes some of the principal period fits giving the peak power and the (peak period)/(predicted period) ratios. The dominant peak fits the $T = 0$ family at the 18.3 km s^{-1} harmonic. There is no significant change in location or power if all the galaxies in common with Croasdale's (1989) original study are deleted. The 18.3 km s^{-1} harmonic, along with 36.6 km s^{-1} and 9.15 km s^{-1} is often strong. The period is also aligned on phase 0.0; the basic periods are simply phased with the CBR rest frame. Perseus data also illustrate the general preference for cube-root families; the $T = 3$ family is distinct. The ninth-root families flanking $T = 6$ are present and match the strong ninth-root family in Virgo. T values do not occur randomly, and there are similarities between samples. Even the low S/N data are consistent. Table 2 shows that when the low quality data are combined with the 28 point sample the longer period $T = 3$ periods are reinforced. The low quality data act as they should; short periods are destroyed but dominant long periods are preserved.

To evaluate the significance of the periodicities we found all the power peaks in excess of 4.0 which fell in the period range 17 to 250 km s^{-1} . The limits are set by the breadth of the power peak at long periods and the growth of noise at short periods. As in Virgo we count the number of matches within a limiting pk/per range and apply binomial statistics. The 53 point sample has 9 fits within 0.004 of unity (1/10 the possible range) and 27 power peaks above 4. The probability of 9 or more hits in 27 trials is only 0.0009 by accident. The 28 point sample has 4 hits out of 9, unlikely at the 0.008 level. If we raise the cutoff period to 36 km s^{-1} to reduce noise the 53 point sample returns 6 hits out of 10, unlikely at the 0.0002 level. The results are consistent with Virgo. Table 3 summarizes some of the binomial test results for both Virgo and Perseus investigations. We again point out that there was no optimization for the wide profile Perseus samples; the samples were defined before equation (9) was discovered.

Following the analysis of the wide profile data the Giovanelli and Haynes (1989) data were examined for narrower profile galaxies. Findings are similar although a limited number of subsamples were studied. Some of the results are given in Table 3. One subsample of the 472 galaxies available used 179 galaxies with $S/N > 4$ and profile widths between 200 and 400 km s^{-1} . A period matching study found 10 of 21 power peaks greater than power 4 falling within 1/5 of the range centered on predicted periods. This returns a random likelihood of 0.004 similar to other such studies. Of special interest is the continuity of the 18.3 km s^{-1} period at $W = 400 \text{ km s}^{-1}$. The lower part of Table 2 shows that the pk/per ratio match is within 1% on both sides, 1.0003 and 1.0002; the power values are 6.9 and 7.1. Such continuity between width intervals, here with a phase shift, is not considered in evaluating significance. Periods are intrinsic to the data, power but not periods can be tuned by selecting profile width intervals. The period is unperturbed here when we make major changes in the width intervals and involve large samples.

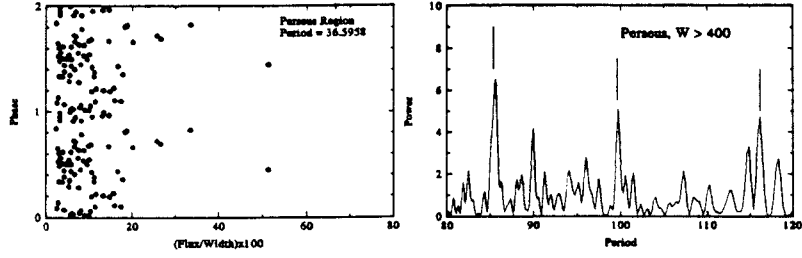


Fig. 4) (left) Phase diagram for Perseus galaxies with wide 21 cm profiles. Points are plotted twice in a double phase cycle at the 36.6 km s^{-1} period. The abscissa is the flux-to-width ratio scaled by 100. There is a regular 18.3 km s^{-1} pattern aligned at phase 0.0 and 0.5. (right) A section of the power spectrum for the 53 point subsample of wide profile Perseus galaxies; W is in km s^{-1} . The abscissa gives periods in km s^{-1} . Three predicted periods are shown with vertical lines. A disproportionate fraction of peaks in excess of power 4 associate closely with predicted periods.

TABLE 2

Spectral Power Data for Perseus

Period km s^{-1}	T	Pk Pow N=53	Pk/Per	Pk Pow N=28	Pk/Per	Pk Pow N=28+73	Pk/Per
36.5958	0	4.4	0.9990
18.2979	0	7.1	1.0003
232.3689	3	5.0	0.9968
116.1845	3	4.8	0.9999
58.0922	3	7.6	0.9984
29.0461	3	4.9	0.9977	4.4	1.0029
99.5984	5	4.9	1.0016
85.3802	7	6.8	1.0029

Comparison Above and Below $W = 400$

V km s^{-1}	W km s^{-1}	S/N (F/W)	N	Pow(Pk/Per) P=18.2979
4500-17500	> 400	(< 0.01)	53	7.1(1.0003)
0-20000	300-400	> 4	76	6.9(1.0002)
0-20000	200-400	> 4	179	6.0(1.0003)

TABLE 3

Binomial Tests of the Distribution of Power Peaks

Sample	N	V km s^{-1}	W km s^{-1}	P km s^{-1}	Fit	Pk>4	Hit	Prob
Virgo	137	All	All	20-100	1/8 1/4	14 14	8 9	0.00008 0.002
Per(W)	53	All	> 400*	17-250	1/10	27	9	0.0009
S/N>4	F/W<0.01*			36-250	1/10	10	6	0.0002
	28	All	> 400*	17-250	1/10	9	4	0.008
	F/W>0.01*							
Per(565)	179	All	200-400	16-250	1/5	21	10	0.004
	31	All	225-250	16-250	1/4	10	7	0.004
	56	6-8000	50-250	10-100	1/16	8	4	0.0009
	34	6-8000	200-350	10-100	1/16	9	3	0.02

* Predetermined

The samples on either side of the $W = 400 \text{ km s}^{-1}$ boundary also provide a good illustration of the stability of the CBR association. Figure 5 shows power maps at the 18.3 km s^{-1} period for a range of the tangential and radial transformation components near the COBE vertex as shown earlier for Virgo. The maps are independent but not significantly different.

5. A Third Sample, The Cancer Supercluster

The deep Arecibo survey of the Cancer region by Bica & Giovanelli (1986ab, 1987) provides an excellent illustration of periodicities. The 643 galaxy study is among the most accurate available. The region provides an especially good illustration of the common $T = 0$ set of periods. For detail see Tift (1996b). The region contains a low redshift foreground where the familiar 36 km s^{-1} periodicity is very apparent from the CBR rest frame. The upper panels in Figure 6 show the 36.6 km s^{-1} phase pattern and power spectrum of the 58 galaxies with redshifts less than 2000 km s^{-1} . Phase is plotted against profile width. The narrow profiles and 36 km s^{-1} period resemble the Virgo galaxies. The power spectrum sharpens and peaks very near the predicted period for the 33 galaxies with $90 < W < 190 \text{ km s}^{-1}$. The lower right panel shows the CBR association for the 33 objects. The first part of Table 4 summarizes the foreground analysis.

The second part of Table 4 shows that the lower redshift end of the Cancer complex, including the Cancer cluster itself, continues the 36.6 km s^{-1} periodicity among the wider profile galaxies. The 18.3 km s^{-1} period dominates when lower luminosity sources are included; the basic 18.3 km s^{-1} period can then be traced through virtually the entire sample of Cancer region objects. Periodicities are not limited to small samples.

The lower left panel of Figure 6 and the last part of Table 4 trace the $T = 0$ periods through the higher redshift data. The 9.15 and 18.30 harmonics alternate as a function of profile width. F/W and S/N levels are set high to show the shorter period clearly. Periods track precisely, usually within 1% of the pk/per range about predictions, through successive independent width intervals while remaining aligned at 0.0 and 0.5 in phase on the 18.3 km s^{-1} scale. Above $W = 400 \text{ km s}^{-1}$ an expanded sample shows the phase break which occurs near $W = 400 \text{ km s}^{-1}$. As found for Perseus data there is no change in period but there is a phase shift. These Cancer data give a clear picture of how phase, harmonics, and width can be interrelated.

6. Short Periods and q_0 Determinations

The analysis of short periods over wide redshift intervals is sensitive to the nonlinearity in z from equation (1). This equation was derived as a Taylor expansion about q_0 of $1/2$ (Tift 1991); the higher order terms permit a determination of q_0 . Short periods in the basic $T = 6$ cube-root family are strong in Perseus, Cancer and local redshift data. They are discussed in Tift (1996b) where we find precise agreement with predicted periods when q_0 is equal to $1/2$. Table 5 contains an example from Perseus and Cancer. The peak power location, near power 10 in these examples, shifts slightly as q_0 is varied. The pk/per ratio passes through 1.00000 when q_0 approaches $1/2$. This result, found for several independent samples, seems extremely unlikely to be accidental. The fit gives considerable confidence in both equations (1) and (9). It is unlikely that a classical interpretation of q_0 is possible in the temporal model.

The determination of q_0 is quite insensitive to the CBR vertex assumed. Figure 7 shows peak power maps as a function of the transverse and radial transformation components. Two large independent samples from the Cancer data are shown; one includes 89 narrow, the other 128 wide profile galaxies. Peak power exceeds 10 close to the standard vertex we have assumed. At this high resolution ($P = 2.88 \text{ km s}^{-1}$) only the edge of the COBE CBR dipole error box is visible at the right.

7. Local Data

The samples so far discussed involve single epoch studies of non-local galaxies, including ones in external superclusters. We now turn to multi-epoch data for local galaxies. We will draw primarily on 21 cm data from the Fisher-Tully (1981) survey from the 70s and data from Tift & Cocke (1988) and Tift (1990)

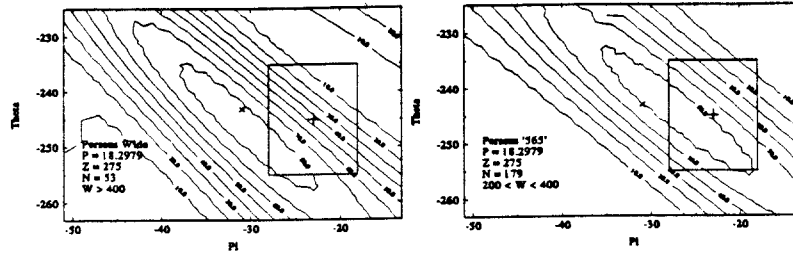


Fig. 5) Contour diagrams of power, at the 18.3 km s^{-1} period, for samples of Perseus galaxies with 21 cm profiles wider and narrower than 400 km s^{-1} . Power is shown scaled by a factor of 10. The axes are the θ and π components, in km s^{-1} , of the vector used to transform to the CBR rest frame. The diagrams refer to a Z component of 275 km s^{-1} . The box is the COBE error box for the CBR dipole vertex; the x is the approximate location of the vertex based upon previous quantization studies. Samples on opposite sides of a phase shift, which occurs near $W = 400 \text{ km s}^{-1}$, define the same vertex.

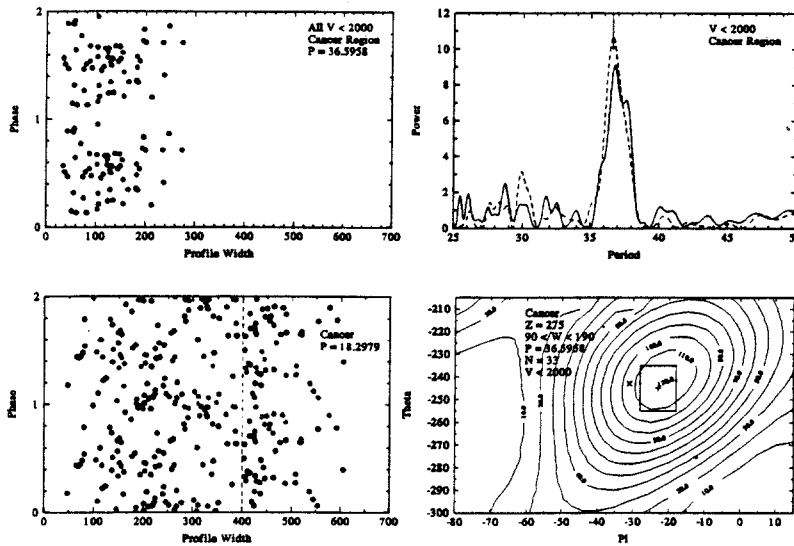


Fig. 6) The left panels show phase-profile width diagrams for Cancer galaxy samples. Phase is plotted in a double cycle. Periods, P , profile widths, W , and redshift, V , are in km s^{-1} . The upper left panel shows the 36.6 km s^{-1} periodicity for low redshift galaxies. The lower left panel shows an alternating periodicity pattern found for higher redshift galaxies when $P = 18.3 \text{ km s}^{-1}$. The selection criterion, discussed in the text, changes at $W = 400 \text{ km s}^{-1}$ where a phase shift occurs. The power spectrum (upper right) refers to the low redshift sample. The solid line is for all 58 low redshift galaxies; 33 galaxies with $90 < W < 190 \text{ km s}^{-1}$ produce the dashed spectrum. A line marks the predicted period. The lower right frame shows the power concentration, for the 33 galaxy set, associated with the CBR dipole vertex. See Figure 5 for a description of axes and symbols.

TABLE 4

Spectral Power Data for Cancer

V km s ⁻¹	W km s ⁻¹	S/N (F/W)	N	Pow(Pk/Per) P=9.1490	Pow(Pk/Per) P=18.2979	Pow(Pk/Per) P=36.5958
0-2000	All	All	58	9.1(1.0043)
	90-190		33	10.7(0.9998)
3500-7000	> 250	> 8	128	...	4.7(1.0023)	7.8(0.9907)
		All	184	...	6.9(1.0027)	...
2000-10000	All		562	...	6.6(1.0022)	...
5000-10000	0-175	(> 0.015)	30	...	4.2(1.0032)	...
	175-275		40	6.7(1.0002)
	275-400		31	...	7.3(1.0000)	...
	0-400		100	8.4(1.0003)
0-10000	> 400	> 8	49	4.3(0.9999)

TABLE 5

Estimation of q_0

Period km s ⁻¹	q_0	Peak	Pk/Per km s ⁻¹	N	V	W km s ⁻¹	F/W km s ⁻¹
5.76348	0.52	5.7626	0.99985	88	4300-17900	>450	<0.015
	0.51	5.7633	0.99997		(-241.5, -24.2, 275.0)		
	0.50	5.7641	1.00011				
	0.49	5.7650	1.00026				
	0.48	5.7659	1.00042				
	0.46	5.7678	1.00075				
2.88174	0.51	2.8815	0.99992	128	3500- 7000	>250	S/N>8
	0.50	2.8818	1.00004		(-241.7, -30.8, 275.1)		
	0.49	2.8821	1.00012				
	0.47	2.8826	1.00030				

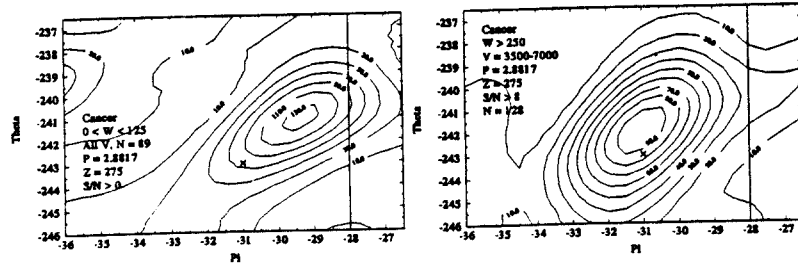


Fig. 7) The power distribution, in the vicinity of the CBR dipole vertex, for two subsets of Cancer region galaxies. W and V give profile width and redshift ranges in km s⁻¹. S/N refers to signal-to-noise limits and N gives the sample size. At the short period shown the power peaks are sensitive to q_0 , and match predicted periods when $q_0 = 0.5$. The independent samples conform closely to the same vertex. See Figure 5 for description of axes and symbols. Only the edge of the COBE error box, the line at right, falls within the frame for such short periods.

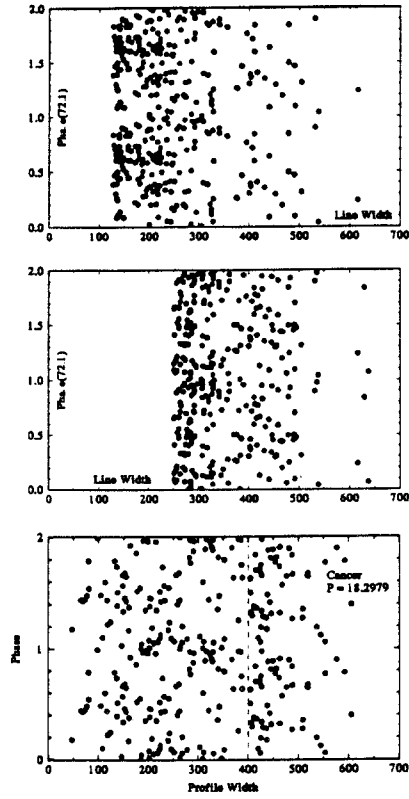


Fig. 8) The upper two frames are phase-width diagrams for local galaxies using Fisher-Tully data; W is in km s^{-1} . The diagrams are from a study of the association of redshift quantization with the CBR rest frame before precise periods were predicted; an empirical 72.1 km s^{-1} period was used. There are distinct periodicities, with a large phase shift, on either side of a transition region near $W = 200 \text{ km s}^{-1}$. The lower frame repeats the Cancer region phase-width diagram from Fig. 6 to show that the same type of transition, involving subharmonics of the period, occurs at this width. The phase shift effect at $W = 400 \text{ km s}^{-1}$ can also be seen in both samples.

from the 80s. Using data from different epochs we can investigate variability. The new data also include quantitative measures of 21 profile shape, the A = asymmetry index. Some material summarized here is from Tift (1996b); details relating to variability will be discussed in Tift (1997).

We find that quantization effects change near certain profile widths. One change occurs near $W = 400 \text{ km s}^{-1}$; a second transition region appears near 200 km s^{-1} . The top two frames of Figure 8 compare one of the original studies of the CBR association using Fisher-Tully galaxies with the lower left frame from the Cancer work in Figure 6. Below $W \approx 175 \text{ km s}^{-1}$ the Fisher-Tully data are periodic. The periodicity then blurs but returns, with a phase shift, by $W \approx 300 \text{ km s}^{-1}$. In the Cancer sample we see the same shift for the basic $18.3 \text{ km s}^{-1} T = 0$ period, and recognize the shift as a transition through the 9.15 km s^{-1} harmonic. The analysis of local galaxies focussed on the $100 < W < 300 \text{ km s}^{-1}$ interval to verify the dominance of $T = 0$ periods and investigate this transition region in detail. Much of the detail is revealed by the way 'deviations', redshift differences between epochs, relate to phase and asymmetry. The main analysis tool is the 'phase-deviation' diagram. Deviation usually refers to the redshift difference Tift & Cocke (1988) minus Fisher-Tully (1981), written TC-FT. The TCF sample contains the 454 galaxies for which this difference is available.

Figure 9 contains phase-deviation diagrams for the TCF sample. The upper left frame includes all 249 galaxies with $100 < W < 300 \text{ km s}^{-1}$. The peak power is above 9 in the CBR rest frame as shown at upper right. The pk/per ratio is 1.0010; the peak falls within the central 2.5% of the range between predicted periods. The well known systematic shift between modern redshifts and Fisher-Tully values is apparent. The lower panels show that periodicity is enhanced by restricting profile asymmetry to less than 10%, and morphology to $t < 9$. The lower right frame also shrinks the width interval. The transition region is not a blur, it contains a finer harmonic structure and is the same in Cancer and locally. S/N has only a small effect; scatter in phase is not due to observational uncertainty, it is due to finer structure. Phase is determined from the modern redshifts; scatter is not much larger than the point size. Scatter in Fisher-Tully redshifts affects deviations only.

To go to still finer structure in the 200 km s^{-1} transition region we must introduce redshift variability. Figure 10 repeats the lower right frame of Figure 9 without a morphology restriction. The vector shows that if a redshift were to decrease by one period between epochs a galaxy could shift from one end of the deviation pattern to the other and remain in phase. This is the type of variability which seems to occur; occasional rapid transitions retain a periodic phasing and generate periodic deviation patterns. There seems to be a secular downward drift; the high redshift end of any level is next in line for change. Intermediate steps may or may not be seen. The lower right frame uses data from galaxies with wider profiles. The frame shows a staggered pattern which would be generated if intermediate levels are occupied. Periodicity in such a case would not be recognized without the deviation information, but a Student's t test comparing deviations in the half phase intervals dividing at .0 and .5 easily shows the periodicity.

The upper right panel of Figure 10 contains the power spectrum of the sample at upper left. The dashed line shows the spectrum without an asymmetry restriction. As with width adjustments, narrowing a parameter range will affect the power, but does not significantly affect periods, the periods are intrinsic to the galaxies. The lower left frame shows the CBR association of the restricted sample. As with periods, restricting the sample does not significantly affect the vertex location. The second peak which appears in the power spectrum matches the $T = 1$ period at 16.94 km s^{-1} . The adjacent ninth root families seem to appear when the cube-root families show evidence of recent or current change. This might be expected if near the beginning or end of a doubling process one axis was out of synchronization with the others.

Asymmetry restrictions appear to improve the resolution of periodicities. If phase scatter is due to the occupancy of intermediate states, asymmetry could be associated with the timing of changes and thus with phase. Figure 11 shows only positively asymmetric galaxies; they concentrate on the wide side of the 200 km s^{-1} transition, populate the $9.149 \text{ km s}^{-1} T = 0$ harmonic and show a sharply staggered pattern consistent with stepwise redshift decay. Objects with $A < 0$ can be shown to favor the narrow side of the 200 km s^{-1} transition zone and shift in phase. In the 0 to -10 km s^{-1} deviation range the $A > 0$ objects show a power, at 9.149 km s^{-1} , in excess of 10. They map into the standard CBR rest frame as shown at upper right. This negative wing is expanded at lower right where points seem to clump laterally at still higher $T = 0$ harmonics. Redshifts seem to change in discrete steps, cascading between relatively stable levels. The sequencing of changes is associated with the width and shape of the 21 cm profiles. The *velocity distribution*

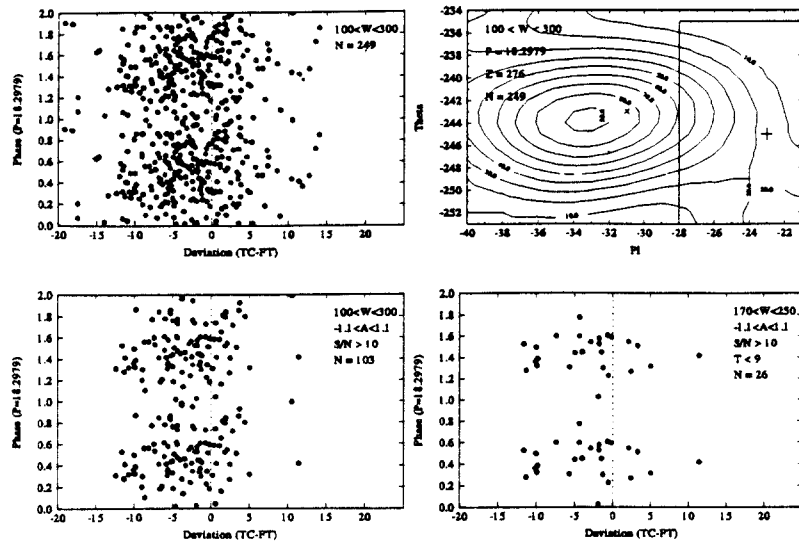


Fig. 9) Three phase-deviation diagrams, and a cosmocentric power map, for local galaxies. The 18.3 km s^{-1} predicted period is used. Deviation is the redshift difference, in km s^{-1} , Tift-Cocke minus Fisher-Tully (a $10 \pm$ year interval). The upper left diagram shows a complete set of 249 galaxies with profile widths, $100 < W < 300 \text{ km s}^{-1}$; points concentrate around phase 0.5. At upper right the association of power with the CBR rest frame is shown. Refer to Fig. 5 for a description of axes and symbols. More restricted samples are shown in the lower frames. Restrictions, in W , profile asymmetry (A index), signal-to-noise, and morphology (t index), improve homogeneity and enhance power, but have no significant affect on the period or vertex location (compare Fig. 10).

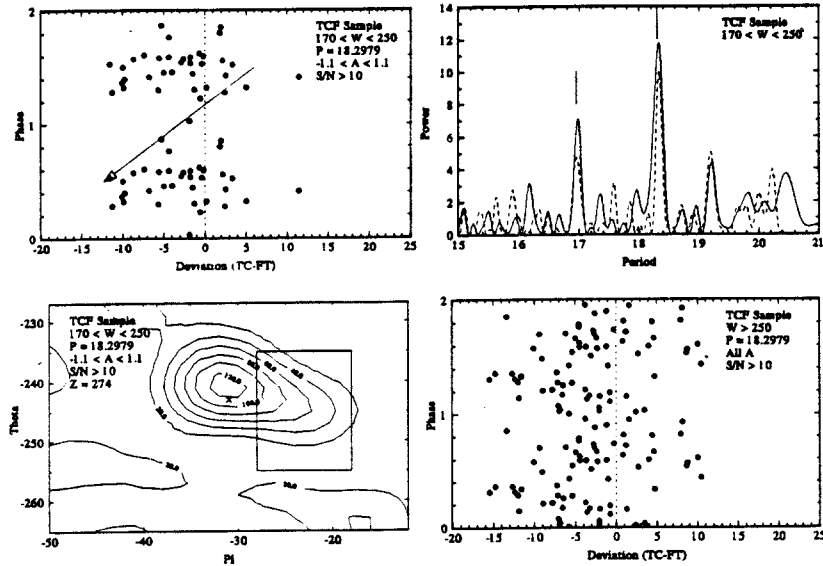


Fig. 10) Redshift variability effects in a restricted sample of local galaxies (see Fig. 9). The vector in the $P = 18.3 \text{ km s}^{-1}$ phase-deviation diagram (upper left) shows how a shift of one cycle between epochs will shift a point, produce a related deviation, and retain the periodicity. In other width intervals, (lower right), intermediate levels seem to occur and a characteristic staggered pattern is seen. The power spectrum (upper right) of the 36-point restricted sample shows a precise period match; predicted periods are marked with lines. Removing S/N and asymmetry, (A), restrictions generates a 92-point sample. Power drops slightly (dashed spectrum) but does not affect the period or CBR association (lower left, see Fig. 5 for a description of axes and symbols). The power spectrum also contains the next shorter predicted period; such periods tend to occur when recent or current variation is suspected.

function determines the transition probabilities. Multiple epoch data and detailed profile shape information are essential for the study or even the detection of redshift variability. It is also apparent that lookback time may cause differences as a function of distance; samples from different redshift ranges cannot be casually combined.

The basic $T = 0$ doubling family appears to dominate the intermediate width profile range and contains mostly normal spirals. Other galaxies seem to fall into three categories. There are two classes of dwarf galaxies with narrow 21 cm profiles, and a general class of wide profile objects. The extreme dwarf galaxies, morphology $t = 9$ or 10 with $W < 75 \text{ km s}^{-1}$, are locally periodic in the $T = 7$ family with a clear asymmetry dependence. This is shown in Figure 12 for all the extreme dwarfs in the TCF sample. Objects with negative asymmetry or symmetric profiles show very strong negative deviations which are periodic at the $10.6726 \text{ km s}^{-1}$ $T = 7$ period. Galaxies with positive asymmetry are phase-shifted as if they lag behind their negative counterparts. This sample, completely independent of the $T = 0$ sample above, shows a clear CBR association and hypothetical transition patterns tuned in absolute phase.

The 10.67 km s^{-1} period and its 5.33 km s^{-1} harmonic were detected prior to the derivation of equation (9) (Tift 1991). Their precise fit into the pattern of predicted periods was one of the major factors which convinced the author of the significance of equation (9). The $T = 7$ ninth-root family bears the same shifted relationship to $T = 6$ as the $T = 1$ periods have with $T = 0$. The presence of shifted ninth-root patterns seems to characterize regions undergoing changes. The $W = 75 \text{ km s}^{-1}$ boundary for this group is not arbitrary; it is the narrow cutoff width for dwarfs found in the original global redshift studies (Tift & Cocke 1984).

Between the extreme dwarfs and the normal spirals of $t = 8$ or earlier, there is a large class of dwarf galaxies. They can be characterized by $t = 9$ or 10 with $75 < W < 250$. These common local galaxies show no overt periodicity until deviations are examined. The $T = 6$ cube-root family of periods then becomes apparent. Figure 13 shows the $46.1078 \text{ km s}^{-1}$ period where the characteristic staggered phase-deviation pattern renders the period visible. A Student's t test, comparing mean deviations in half phase intervals dividing at .0 and .5, indicates that the segments have only an 0.001 chance of being from the same deviation distribution. One interval shows no deviation; the other deviation is consistent with the 5.7635 km s^{-1} $T = 6$ period, a subharmonic of the 46 km s^{-1} period. This class of objects is particularly interesting since recent observations alone show changes. The right panel of Figure 13 compares galaxies of the same general type using 1984 and 1986 observations. The same periodic wave is present with a low amplitude consistent with the short time interval involved. It seems that whatever shift occurred was still in progress in 1984; evidence for variability is not limited to Fisher-Tully data. Larger consistent shifts for spirals can also be demonstrated using some of the oldest available 21 cm data.

The wide profile galaxies show a very strong 5.7635 km s^{-1} $T = 6$ periodicity. This is illustrated in Figure 14, first for a restricted class of symmetric profile galaxies with $W > 250 \text{ km s}^{-1}$, then for the unrestricted sample of all objects with $W > 200 \text{ km s}^{-1}$. A characteristic staggered pattern is present with the negative wing aligned precisely on phase 0.0. The power spectrum of the galaxies in the deviation interval from -2 to -8 km s^{-1} peaks at power 17 for $P = 5.7631$ for the 36 symmetrical profiles, and at power 16.3 for $P = 5.7624$ for all 64 objects. The period is matched within one-half of one percent of the P_k/P_{er} range, shows extraordinary power, and is aligned and in phase with the CBR rest frame.

Sample adjustments have no significant effect on power, period or the CBR association shown at lower right. This same periodicity is clear in the wide profile Perseus galaxies, and its harmonic in the wide-profile Cancer galaxies; these periodicities were among those used to determine q_0 . The short $T = 6$ periods appear to be quite universally present among the wide profile galaxies. The $T = 0$ family dominates in galaxies with intermediate profile widths, then longer period $T = 6$ periods return among the dwarfs. The extreme dwarfs shift to the adjacent $T = 7$ family. Specific classes of galaxies associate with different T values and dominant period ranges; the $T = 0$ and $T = 6$ cube-root families stand out. Periods are not randomly distributed in T . Table 6 summarizes the major sets of periods.

8. The Relationship Between the CBR and Galactocentric Frames

One of the puzzles posed by redshift quantization is the presence of two significant rest frames. As a first step in trying to understand this duality we believe that it is necessary to abandon the idea that galaxies

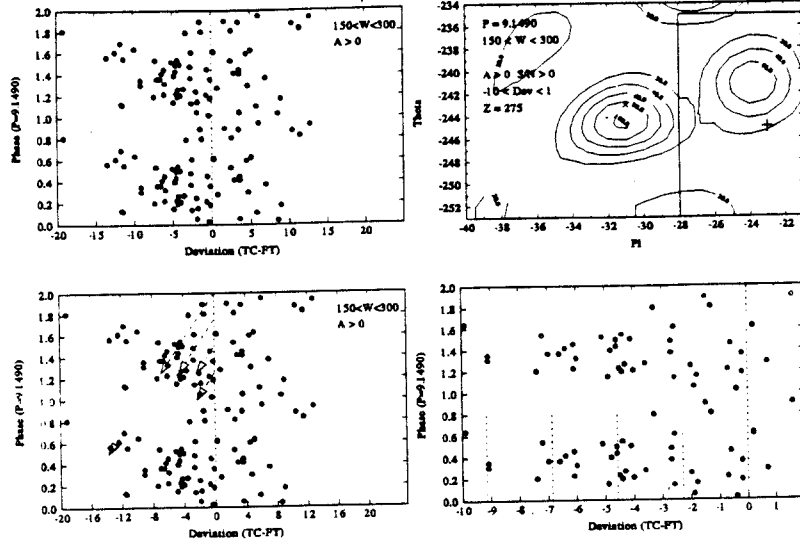


Fig. 11 Phase-deviation diagrams and a power contour map for local galaxies with positive asymmetry and profile widths in the upper portion of the $100 < W < 300 \text{ km s}^{-1}$ transition region. A strong negative deviation is present and periodic at 9.15 km s^{-1} . The pattern is consistent with discrete changes (lower left) involving a substructure at still higher harmonics (lower right). Power contours for galaxies with $-10 < \text{dev} < -1 \text{ km s}^{-1}$ (upper right, see Fig. 5 for a description of axes and symbols) show power in excess of 10 very close to the adopted CBR dipole vertex.

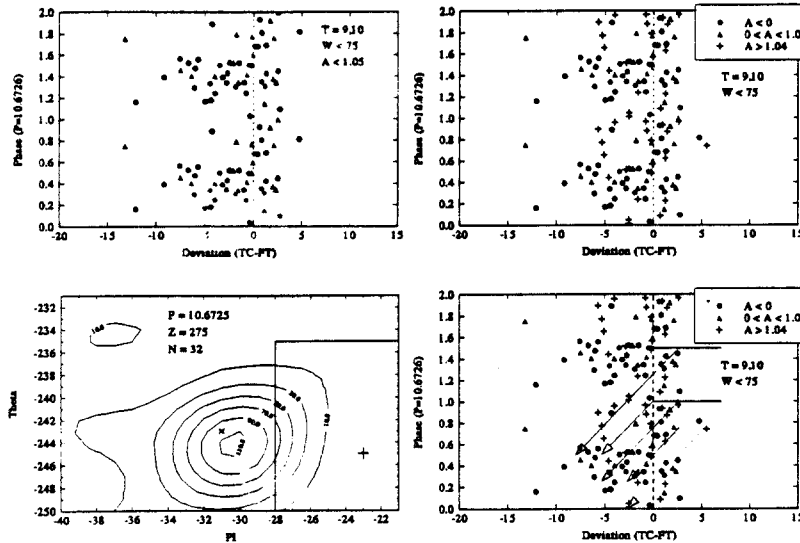


Fig. 12 Phase-deviation diagrams and power contours for local galaxies with extreme dwarf characteristics, $t = 9, 10$ and $W < 75 \text{ km s}^{-1}$. A strong negative deviation is present for galaxies with symmetric and negatively asymmetric 21 cm profiles (upper left). The period is 10.67 km s^{-1} , shifted one ninth-root cycle from the common $T = 6$ family of periods. Galaxies with positively asymmetric profiles, are phase shifted (upper right). The pattern is consistent with discrete changes (lower right) where asymmetry distinguishes between stages. Power contours for the negative wing of galaxies (upper left) show power in excess of 11 very close to the adopted CBR dipole vertex (lower left, see Fig. 5 for axes and symbols)

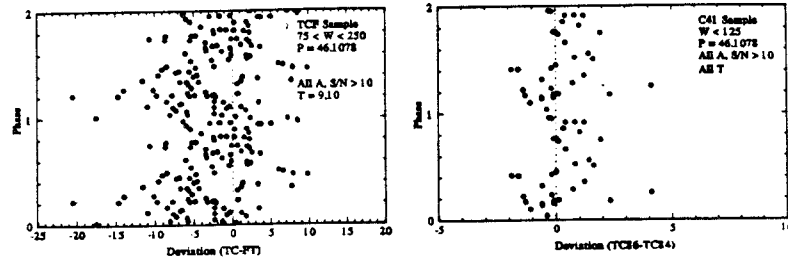


Fig. 13 Phase-deviation diagrams for local dwarf galaxies; a staggered deviation pattern, associated with variability, occurs at the 46.1 km s^{-1} period. The comparison between modern redshifts and Fisher-Tully data is shown at left for galaxies with $t = 9, 10$ and $75 < W < 250 \text{ km s}^{-1}$. The pattern continued to develop between 1984 and 1986 as shown for dwarf galaxies with $W < 125 \text{ km s}^{-1}$ at right. The deviation scale, in km s^{-1} , is expanded by a factor of 3 in the right frame.

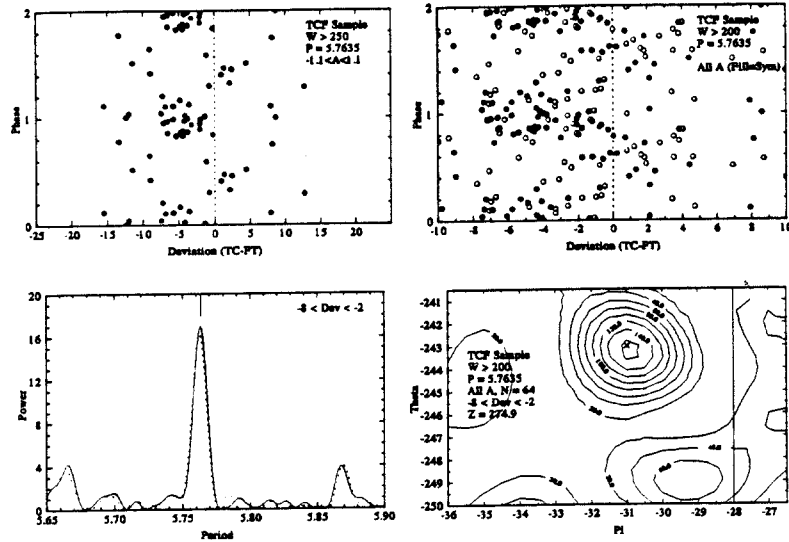


Fig. 14 Phase-deviation diagrams, power spectra and power contours for local supercluster spirals with wide 21 cm profiles. Galaxies with $W > 250 \text{ km s}^{-1}$ and symmetric profiles (upper left) show a distinct staggered pattern of deviations at the 5.76 km s^{-1} period. This period is almost universally present in galaxies with wide 21 cm profiles. Deviations between -8 and -2 km s^{-1} are aligned on phase 0.0 and achieve a power of 17 (lower left) precisely at the predicted period. When asymmetry restrictions are removed and the W range lowered to 200 km s^{-1} to maximize the sample (upper right) there is no significant change of power or period (dashed line in spectrum). The power peak occurs at the adopted CBR dipole vertex (lower right, see Fig. 5 for axes and symbols)

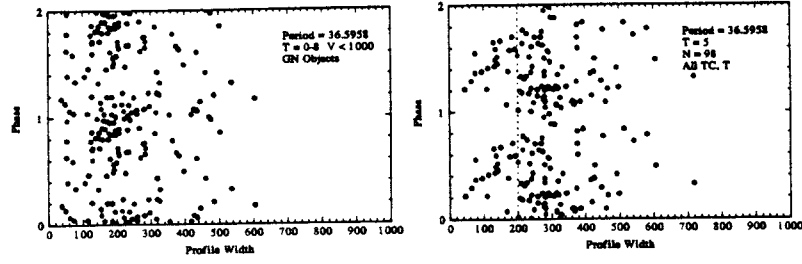


Fig. 15) Phase-profile width diagrams, in the galactocentric rest frame, for spiral galaxies. The basic 36.6 km s^{-1} period is used; W is in km s^{-1} . The left frame contains a 106 point Guthrie-Napier sample of nearby spirals. These very local objects are periodic but are heavily dwarf dominated. The right frame contains 98 classical Sc ($t = 5$) galaxies. The periodicity is again detectable in specific width intervals, but is not phased with other types and shows a distinct change near $W = 200 \text{ km s}^{-1}$. Such periodicities, much more regular in the CBR rest frame, appear to induce strong periodic fluctuations in local galaxy samples observed in the galactocentric frame.

move about in space with respect to one another. Such motion for our Galaxy can explain the CBR dipole observation, but combined with similar random motions for other galaxies would destroy global quantization. If we accept quantization we require a non-velocity explanation of the CBR transformation. In the temporal model, described elsewhere, galaxies are quantized structures dispersed, and evolving, in three-dimensional time. In the model the CBR transformation places the observer in the quantized frame associated with 3-d temporal space. We see quantized patterns which depend only on lookback time and the characteristics of the particular type of galaxies we choose to observe.

At the same time we cannot overlook the fact that within our Galaxy we have real spatial motion with respect to the galactic center. When we apply the galactocentric transformation we remove this motion, but this is not sufficient to place us in the quantized temporal frame. As a 3-d temporal object the Galaxy has certain properties; the CBR transformation removes these along with the spatial solar motion. The galactocentric transformation removes only the spatial part. This seems to be sufficient to induce local resonant patterns which appear as intense fluctuations rather than a regular global pattern.

The two transformations appear to be linked in two of the components; within scatter in local random stellar motions the tangential components are equal and opposite (-243 and $+232$ km s^{-1}) while the radial terms are the same, (-31 and -36 km s^{-1}). In the temporal model the dynamics of a galaxy may be associated with the temporal structure. This seems to have the effect of placing the CBR vertex nearly opposite the galactocentric one in longitude. The transformation terms in longitude simply change sign. Given the intense tuning present in the CBR frame one might expect to see resonances opposite the longitude of the CBR vertex if only the spatial correction is done. This is especially true if one looks at classes of galaxies with similar temporal properties.

Figure 15 (left) takes the sample of local spirals, $V < 1000$ km s^{-1} , used by Guthrie and Napier (1991), and refers them to the galactic center for the predicted 36.6 km s^{-1} period. The phase-width diagram identifies the galaxies as dwarf objects; there are few major galaxies involved. This set of galaxies is similar enough internally that just the removal of the dynamical motion correction reveals the periodicity. This is also true in the right frame where the entire set of Sc galaxies ($t = 5$) with recent Tift-Cocke or Tift redshifts is shown. These extend much further in redshift, show the basic periodicities at 36.6 and 18.3 km s^{-1} , and the 200 km s^{-1} profile width transition. They are obviously not in phase with the local dwarf objects, however. Given such periodic clumping any fairly local sample should be far from random in its redshift distribution. A search around the galactic center, or the anti-longitude of the CBR vertex, should detect strong fluctuations.

Such a search was carried out using a recent 104 point set of spirals defined by Guthrie and Napier. Figure 16 shows the locations of strong power peaks for an 18.8 km s^{-1} period related to the Guthrie and Napier findings. There is an intense pattern of power peaks concentrated around the anti-longitude of the CBR dipole vertex (shown as a cross). Our standard galactocentric vertex is shown with an X. The triangles are the locations of strong 37 km s^{-1} periodicities recently mapped by Guthrie and Napier (1996). Because of the close proximity of the galactocentric vertex and the CBR anti-longitude point, it may be difficult to separate galactic and CBR correlations. We suspect that all or most galactocentric findings can be traced back to the cosmocentric effect through the intimate connections between the two transformations.

9. Summary

In 1992 and 1993 redshift quantization was associated with the CBR rest frame, and a model involving 3-d time was developed which permits precise predictions of possible global periodicities. Two basic equations now exist, one to linearize periodicities in z , and the other to define periodicities. These are:

$$V_{corr} = 4c[(1+z)^{1/4} - 1] + \dots \quad \text{and} \quad P = c2^{-\frac{9D+T}{9}}. \quad (10)$$

The equations are consistent with a model combining 3-d time with 3-d space within which fundamental particle properties at one extreme, and cosmological observations at the other, may be related. The following statements summarize and expand on the characteristics of the redshift introduced in Section 3.

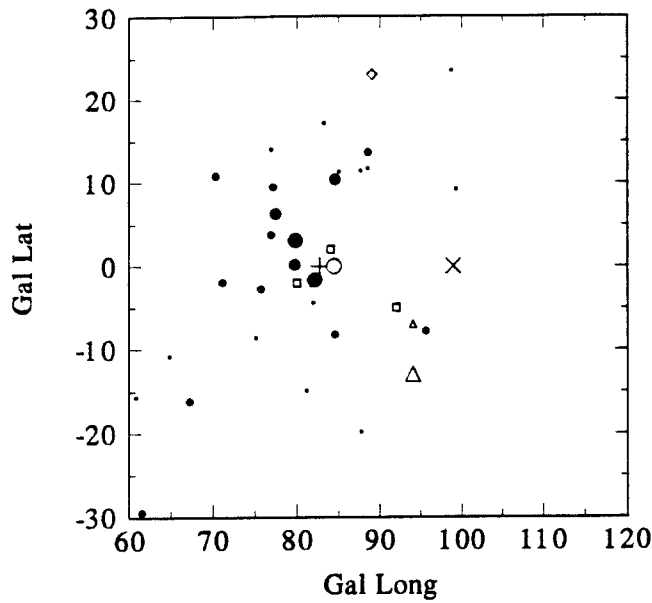


Fig. 16 Locations of power peaks, in galactic coordinates, for 104 local supercluster galaxies examined recently by Guthrie and Napier. An X marks the standard galactocentric quantization vertex; the cross and open circle mark points, in the galactic plane, opposite the longitude of the cosmocentric quantization and COBE vertices. Large power fluctuations (filled symbols) at $P = 18.8 \text{ km s}^{-1}$, half of the 37.5 km s^{-1} period studied by Guthrie and Napier, associate with the anti-CBR point. Power varies from 9 for the smallest symbols to 17 for the largest. They were found in a 10^6 point search through a velocity cube using a 2 km s^{-1} resolution. Open symbols identify other periodicities found by Guthrie and Napier. These features occur at frequencies greatly in excess of random expectations and are believed to be local fluctuations induced by a basic cosmocentric pattern.

TABLE 6

Selected Redshift Periods $P = c2^{-\frac{2D+T}{9}}$					
$D \backslash T$	7	6	5	1	0
17	2.2872
16	2.6681	2.8817	4.5745
15	5.3363	5.7635	9.1490
14	10.6725	11.5270	...	16.9416	18.2979
13	33.8831	36.5958
12	...	46.1078	49.7992	...	73.1916
11	...	92.2157	99.5984	...	146.3833
10	...	184.4313

- 1) Width, redshift range, and profile asymmetry adjustments influence spectral power but do not tune periods. As parameters are varied, power may shift between periods, especially harmonics within one T family, but peaks closely track predicted periods.
 - 1a) Distinct phase shifts within the same period occur near certain profile widths. These shifts involve steps through subharmonics which suggests that real transitions in redshift occur from time to time. Patterns of offset redshift deviations between different epochs are consistent with such changes.
 - 1b) Redshifts concentrate in absolute phase around simple fractions of the periods. Concentrations are not randomly spread in phase.
- 2) The pk/per ratio is a measure of the quality of fit to the set of predicted periods. Power peaks concentrate strongly around 1.00 and avoid values near 1.04 midway between predictions. Short periods at high redshifts indicate that $q_0 = 1/2$.
- 3) Certain periods or T values tend to associate with particular morphology and profile width intervals. Four major classes have been identified in local redshift data. Periods in the basic $T = 0$ family are almost always dominant.
 - 3a) Periods are not distributed randomly in T ; two cube root families, $T = 0$ and 6, dominate. Ninth-root families often associate with the dominant families, $T = 1, 5$ and 7 being the most important. Table 6 summarizes common periods associated with classes of galaxies.
- 4) Power at predicted periods is maximized when redshifts are transformed to a rest frame close to the COBE CBR vertex. The radial component is slightly more negative than the COBE value. The galactocentric rest frame seems to be intimately related to the CBR frame.

Acknowledgements

The author is very much indebted to John Cocke who was instrumental in the derivation of equation (1) and the pursuit of the CBR connection. The author is also especially indebted to Ari Lehto for his pioneering work in developing 3-d temporal concepts, particularly those relating to the description of fundamental particles. Carl DeVito and Anthony Pitucco have also contributed numerous basic ideas which assisted appreciably in development of the current 3-d temporal model.

References

- Bicay, M. D., & Giovanelli, R. 1986a, *AJ*, 91, 705
 Bicay, M. D., & Giovanelli, R. 1986b, *AJ*, 91, 732
 Bicay, M. D., & Giovanelli, R. 1987, *AJ*, 93, 1326
 Cocke, W. J., & Tift, W. G. 1996, *Astroph. & Space Sci.*, in press
 Cocke, W. J., DeVito, C., & Pitucco, A. 1996, this conference
 Croasdale, M. R. 1989, *ApJ*, 345, 72
 Fisher, J. R., & Tully, R. B. 1981, *ApJS*, 47, 139
 Giovanelli, R., & Haynes, M. P. 1985, *AJ*, 90, 2445
 Giovanelli, R., & Haynes, M. P. 1989, *AJ*, 97, 633
 Guthrie, B. N. G., & Napier, W. N. 1991, *MNRAS*, 253, 533
 Guthrie, B. N. G., & Napier, W. N. 1996, *A&A*, in press
 Hoffmann, G. L., Helou, G., Salpeter, E. E., Glosson, J., Sandage, A. 1987, *ApJS*, 63, 247
 Lehto, A. 1990, *Chinese J. Phys.*, 28, 215
 Tift, W. G. 1978a, *ApJ*, 221, 449
 Tift, W. G. 1978b, *ApJ*, 221, 756
 Tift, W. G. 1990, *ApJS*, 73, 603
 Tift, W. G. 1991, *ApJ*, 382, 396
 Tift, W. G. 1995a, *Astroph. & Space Sci.*, 227, 25

Tift, W. G. 1995b, *Mercury*, 24, 12
Tift, W. G. 1996a, this conference
Tift, W. G. 1996b, *ApJ*, in press (Sept. 10)
Tift, W. G. 1997, in preparation
Tift, W. G., & Cocke, W. J. 1984, *ApJ*, 287, 492
Tift, W. G., & Cocke, W. J. 1988, *ApJS*, 67, 1
Tift, W. G., Cocke, W. J., & DeVito, C. 1996, *Astroph. & Space Sci.*, submitted
Tift, W. G., & Lehto, A. 1996, in preparation